Published in final edited form as:
J Comp Neurol. 2011 February 1; 519(2): 194–210. doi:10.1002/cne.22509.

Stereocilin connects outer-hair-cell stereocilia to one another and to the tectorial membrane

Elisabeth Verpy[1,2,3,4,*], **Michel Leibovici**[1,2,3,4,†], **Nicolas Michalski**[1,2,3,4], **Richard J. Goodyear**[5], **Carine Houdon**[1,2,3,4], **Dominique Weil**[1,2,3,4], **Guy P. Richardson**[5,#], and **Christine Petit**[1,2,3,4,#]

[1] Institut Pasteur, Unité de Génétique et Physiologie de l'Audition, F75015 Paris, France.

[2]Inserm UMRS 587, F75015 Paris, France.

[3]Collège de France, F75015 Paris, France.

[4]Université Pierre et Marie Curie, F75015 Paris, France.

[5]University of Sussex, School of Life Sciences, Falmer, Brighton BN1 9QG, UK.

Abstract

Stereocilin is defective in a recessive form of deafness, DFNB16. We studied the distribution of stereocilin in the developing and mature mouse inner ear and analyzed the consequences of its absence in stereocilin-null (*Strc*$^{-/-}$) mice that suffer hearing loss starting at post-natal day 15 (P15) and progressing until P60. Using immunofluorescence and immunogold electron microscopy, stereocilin was detected in association with two cell surface specializations specific to outer hair cells (OHCs) in the mature cochlea: the horizontal top connectors that join the apical regions of adjacent stereocilia within the hair bundle, and the attachment links that attach the tallest stereocilia to the overlying tectorial membrane. Stereocilin was also detected around the kinocilium of vestibular hair cells and immature OHCs. In *Strc*$^{-/-}$ mice, the OHC hair bundle was structurally and functionally normal until P9. Top connectors, however, did not form and the cohesiveness of the OHC hair bundle progressively deteriorated from P10. The stereocilia were still interconnected by tip links at P14, but these progressively disappeared from P15. By P60, the stereocilia, still arranged in a V-shaped bundle, were fully disconnected from each other. Stereocilia imprints on the lower surface of the tectorial membrane were also not observed in *Strc*$^{-/-}$ mice, thus indicating that the tips of the tallest stereocilia failed to be embedded into this gel. We conclude that stereocilin is essential to the formation of horizontal top connectors. We propose that these links, which maintain the cohesiveness of the mature OHC hair bundle, are required for tip-link turn over.

Keywords

inner ear; cochlea; organ of Corti; hair-bundle cohesiveness; horizontal top connectors; attachment links

[*]Correspondence to: Unité de Génétique et Physiologie de l'Audition, Institut Pasteur, 25 rue du Dr Roux, 75724 Paris Cedex 15, France. Phone : 33 1 40 61 36 52. Fax : 33 1 40 61 34 42. elisabeth.verpy@pasteur.fr. .
[†]Present address: Institut Cochin, Inserm U1016, CNRS UMR8104, F75014 Paris, France.
[#]These authors contributed equally to the work.

Europe PMC Funders Author Manuscripts

Introduction

Two types of sensory cells, the inner and outer hair cells (IHCs and OHCs, respectively) are housed in the auditory epithelium of the mammalian cochlea, the organ of Corti. This organ is sandwiched between a sheet of paucicellular connective tissue, the basilar membrane, and an overlying acellular gel, the tectorial membrane (TM). Sound-induced vibrations of the organ of Corti stimulate the mechanosensitive sensory cells' hair bundle, which is composed of modified microvilli, the stereocilia. Deflections of the hair bundle open tension-gated ion channels, which produces a receptor potential in the hair cell. IHCs are considered to play a purely sensory role, encoding and transmitting information via the cochlear nerve fibers to the brainstem auditory nuclei. In contrast, OHCs act as cochlear amplifiers that feed energy back into the motion of the organ of Corti. At low sound pressure levels, this boosts the sound-evoked displacement of the basilar membrane, thereby conferring the cochlea with its remarkable sensitivity. Two processes in OHCs have been proposed to be the cellular sources of the amplification: somatic motility (electromotility), length changes of the lateral wall of the OHC driven by the receptor potential (Brownell et al., 1985; Ashmore, 1987), and "active" hair bundle motility (Kennedy et al., 2005) driven by the gating of the mechano-electrical transducer channels. As amplification is frequency selective, OHCs also contribute to the sharp tuning of the cochlea. The non-linear behavior of OHCs results in suppressive masking interactions (one tone suppresses or softens another) that contribute to speech intelligibility (Delgutte, 1996), and introduces strong waveform distortion (Goldstein, 1967). Distortion produces sounds with frequencies not present in the acoustic stimulus that can be re-emitted by the cochlea into the ear canal. These sounds compose the distortion-product otoacoustic emissions (DPOAEs) (Kemp, 1978), which are extensively used to test the auditory function in newborns.

The stereocilia of the sensory hair bundles are arranged in rows of graded heights and are grouped into a tight unit. In the differentiating hair bundle, a genuine cilium, the kinocilium, is also present. The IHC bundle is free standing in the subtectorial space and thought to be deflected by the sound-induced local motion of the endolymphatic fluid. In contrast, the OHC bundle is attached to the TM. As a result, the OHC bundle is deflected by the sound-evoked, relative displacement of the proximal and distal insertions of its stereocilia into the cuticular plate (a dense network of actin filaments at the apex of the cell body) and the TM, respectively. Hair bundles of all vestibular hair cells are also embedded in overlying acellular gels (the otoconial membranes in the saccule and utricle, and the cupula in the ampullae of the semi-circular canals), mainly by means of their kinocilium that persists throughout life.

In the OHC hair bundle, only the tips of the tallest stereocilia are embedded in the TM. The hair bundle operates as a single functional unit and the mechano-electrical transducer channels are gated in a concerted fashion (Kozlov et al., 2007). Forces applied to the tallest stereocilia row must therefore be shared by all stereocilia. This distribution of the forces through the OHC hair bundle is likely to involve inter-stereocilia links, i.e. the tip link that extends from the tip of a stereocilium to the side of the adjacent taller stereocilium and is thought to gate the transducer channel, as well as the lateral links that connect the adjacent stereocilia laterally, both within and between rows. Different types of lateral links have been described in the developing and mature OHC hair bundle (Goodyear et al., 2005). In the mature OHC, these links, called horizontal top connectors or side links, connect the upper parts of stereocilia. They are grouped in bands which have a zipper-like appearance, due to the presence of a central density (Furness and Hackney, 1985; Osborne et al., 1988; Tsuprun and Santi, 2002).

Stereocilin is a protein that is defective in a recessive form of deafness, DFNB16 (Verpy et al., 2001). Stereocilin-null mutant mice have a progressive hearing loss developing from P15 onwards, with auditory thresholds above 10 kHz increasing from 25 dB at P15 to 60 dB at P60. Suppressive masking and both acoustic and electrical waveform distortions are lacking in these animals, whatever the developmental stage, even at P14 when cochlear sensitivity and frequency selectivity are still normal. This unique functional situation has been attributed to the absence of the horizontal top connectors, structures with which stereocilin is associated in wild-type mice (Verpy et al., 2008). Here, we analyze the distribution of stereocilin in the developing cochlea and vestibular end organs of the mouse, and we investigate the effects of the absence of stereocilin on the development of the OHC hair bundle and its coupling to the TM.

MATERIAL AND METHODS

METHODS

Animals—*Cdh23*$^{v2j/v2j}$ and *Pcdh15*$^{av3j/av3j}$ mice were obtained from Jackson Laboratories (Bar Arbor, ME). The *Cdh23*^{v2j} allele carries a donor splice site mutation. All the aberrant transcripts produced from this allele contain a premature stop codon (Di Palma et al., 2001). In the *Pcdh15*^{av3j} allele, insertion of a nucleotide after position 4521 in the coding region results in a frameshift and a premature stop codon. Any encoded protein is predicted to lack a cytoplasmic domain (Alagramam et al., 2001). *Myo7a*$^{4626B/4626B}$ mice were kindly provided by Dr K. P. Steel (Sanger Institute, Cambridge, UK). In these mice, a C to T transition results in a glycine to stop codon change at position 720 of the encoded protein and immunoblot analysis showed that there is less than 1% of the normal level of the protein (Mburu et al., 1997). We produced the *Tecta*$^{\Delta ENT/\Delta ENT}$ (Legan et al., 2000), *Strc*$^{-/-}$ (Verpy et al., 2008), *Ush1c*$^{-/-}$ (Lefèvre et al., 2008), and the *Ush1g*$^{-/-}$ knockout mice (Caberlotto *et al.*, manuscript in preparation). The targeted deletion of exon 2 in *Tecta* is predicted to cause a deletion of 96 amino acids in α-tectorin. The protein is not detected by western-blot analysis in the cochlea of P2 *Tecta*$^{\Delta ENT/\Delta ENT}$ mice. Targeted deletion of exons 2 and 3 in *Strc* results in a frameshifting deletion that would produce an incomplete signal peptide followed by 30 out-of-frame aminoacids. *Ush1c* was inactivated by targeted deletion of exon 1. Consistent with exon 1 containing the transcription start site for every known harmonin mRNA, no *Ush1c* transcripts were detected in inner ears from *Ush1c*$^{-/-}$ mice. The *Ush1g*$^{-/-}$mice were obtained by targeted deletion of exon 2 in *Ush1g*.

The distribution of stereocilin was studied in Swiss mice during development and in adult Hartley albino guinea pigs.

Animal experiments were carried out in accordance with the “Institut de la Santé et de la Recherche Médicale (INSERM)” animal welfare guidelines, approved by the French “Ministère de l’Alimentation, de l’Agriculture et de la Pêche”.

Antibody characterization—Please see Table 1 for a list of the antibodies used. The two anti-stereocilin rabbit polyclonal antibodies, anti-B and anti-D have already been reported (Verpy et al., 2008). They have been produced against synthetic peptides B (NH_2-970-CFLSPEELQSLVPLSD-COOH) and D (NH_2-1753-EQLAYLSPEQRRAVA-COOH) derived from the amino-acid sequence of mouse stereocilin. The antibodies were affinity-purified on the corresponding peptides, and their specificity was verified by immunoblotting and immunostaining of transfected cells (HeLa, Cos7, MDCK) producing full-length stereocilin, and by the loss of inner-ear immunolabeling in *Strc*$^{-/-}$ mice. Both antibodies gave similar staining patterns, but immunolabeling with anti-D required a pretreatment with methanol (Triton X-100 was ineffective), which precluded subsequent phalloidin staining. The results presented are those obtained with the anti-B antibody.

Immunolabeling studies—For immunofluorescence detection, we used Alexa Fluor 488-conjugated goat anti-rabbit F(ab')$_2$ IgG fragment (1:800, Molecular Probes). Anti-acetylated tubulin 6-11B-1 (Sigma/Aldrich) was used at 1:300 final dilution and detected using Cy3-conjugated sheep anti-mouse IgG (1:800, Amersham). Actin was labeled using TRITC-conjugated phalloidin (1 μg/ml, Sigma/Aldrich). For whole-mount preparations, vestibular and cochlear sensory areas were dissected and processed as described (Verpy et al., 2008). Whole-mount preparations and 40 μm thick cryostat tissue sections were analyzed with a laser scanning confocal microscope (LSM-510 META, Zeiss). The first steps of immunolabeling for SEM were done as for immunofluorescence detection. Primary antibodies were detected with protein A-conjugated 15 nm colloidal gold particles (EM Lab, Utrecht, The Netherlands; diluted 1/60 in phosphate buffered saline (PBS) containing 1% serum albumin). Finally, samples were post-fixed in 2.5% glutaraldehyde in PBS for 1 hour before proceeding to SEM.

Transmission electron microscopy—For immunogold electron microscopy, pre-embedding labeling using the anti-B antibody was done as described (Michel et al., 2005). Procedures for transmission electron microscopy were as described (Goodyear et al., 2005).

Scanning electron microscopy—Inner ears were fixed in 2.5% glutaraldehyde in PBS for at least 1 hour. The sensory areas were microdissected, dehydrated in graded ethanol solutions, and critical-point dried from liquid CO_2. Specimens were then mounted on aluminium stubs with colloidal silver adhesive and sputter-coated with gold palladium before imaging in a JSM-6700 F Jeol scanning electron microscope. When immunolabeling was coupled to SEM, dried specimens were mounted on colloidal silver adhesive (Quick drying silver paint, Agar Scientific) to enhance their conductivity. Specimens were then coated with 30 nm of carbon and imaged using a Yttrium Aluminium Garnet (YAG) back-scatter detector.

Electrophysiological studies—Recordings of mechanoelectrical currents in hair cells were performed as described previously (Michalski et al., 2007).

Illustration production—All illustrative images were cropped and adjusted for contrast and brightness using Photoshop CS3 (Adobe Systems, San Jose, CA), and were arranged and labeled using Illustrator CS3 (Adobe Systems, San Jose, CA).

RESULTS

Stereocilin in the vestibular and cochlear hair bundles

We used two affinity-purified polyclonal antibodies, anti-B and anti-D, raised against unique peptide sequences (see Methods) to study the distribution of stereocilin in the mouse inner ear. The two antibodies gave the same pattern of immunostaining, and staining was not observed in stereocilin-null mice.

In the vestibule, stereocilin was detected along the kinocilium of every hair cell (Fig. 1) from embryonic day 15.5 (E15.5) onwards. The immunostaining was restricted to the kinocilium on thick cryostat tissue sections (Fig 1a-1c), but extended far beyond the kinocilium in whole-mount preparations, in a fibrillar pattern (Fig. 1d-1g) that remained associated with the overlying acellular gels when they were detached (Fig. 1h, i).

Cochlear differentiation progresses from the base to the apex of the organ. Stereocilin was first detected along the kinocilium of OHCs at postnatal day 2 (P2). The kinocilium of IHCs was not labeled, although a labeling above the IHC surface in the kinocilium region was

occasionally present (Fig. 2a). At P3, a V-shaped immunoreactivity also appeared at the tip of the hair bundle in all 3 rows of OHCs from the basal-end of the cochlea (not shown). By P7, stereocilin was detected in the hair bundles of OHCs throughout the cochlea, and was restricted to the tallest row of stereocilia (Fig. 2b). Between P10 and P12, three V-shaped stacks of labeling became apparent in each hair bundle, with stereocilin progressively appearing in the middle and then the short row of stereocilia (Fig. 2c, d). In contrast, the hair bundles of IHCs were not immunoreactive (Fig. 2b, 2e). The apical OHCs from adult guinea pigs have tall hair bundles and were therefore expected to allow a more accurate stereocilin localization along stereocilia (Fig. 2f). In this species, the staining in the tallest row of OHC stereocilia was restricted to the distal end of each stereocilium. In the middle and the short rows, stereocilin immunoreactivity was more broadly distributed. In particular, it could be unambiguously localized below the stereocilia tips in the middle row, a distribution reminiscent of that of horizontal top connectors.

Stereocilin was also detected on the undersurface of the TM. In the basal cochlear turn at P5, regularly-spaced immunoreactive spots matched the positions of the kinocilia from the third row of OHCs (Fig. 2g). Remarkably, in the facing epithelium, these kinocilia, which could still be visualized using acetyl-tubulin labeling (data not shown), were no longer stained by the anti-stereocilin antibodies, thus indicating that stereocilin was largely associated with the overlying TM. At P7, both the kinociliary spots and the single V-shaped stack of stereocilin immunoreactivity from the third and second rows of OHCs became associated with the TM (Fig. 2h). From P8 onward, three parallel rows of single stereocilin-immunoreactive V-shaped imprints, one from each OHC, were present on the undersurface of the TM (see stage P15 on Fig. 2i). In adults, this single V-shaped immunostaining of the TM persisted but was fainter than at P15 and displayed a gradient of intensity, decreasing from the base (faint) to the apex (undetectable) of the cochlea.

Stereocilin is associated with both the tectorial membrane attachment links and the interstereociliary links

We used immunogold labeling to detect stereocilin in OHCs by transmission (TEM) and scanning (SEM) electron microscopy in the mature cochlea. Using TEM, stereocilin was detected around the tips of the stereocilia from the tallest row (Fig. 3a) and in association with the top connectors that connect adjacent stereocilia within and between rows (Fig. 3b). Using SEM, in addition to the labeling between adjacent stereocilia, especially in the middle and short rows of stereocilia, we saw gold particles forming a ring around the tip of each stereocilium in the tallest row of stereocilia (Fig. 3c, d), as reported (Verpy et al., 2008). Remarkably, a similar ring of gold particles surrounded the imprints produced by the tall stereocilia on the lower surface of the TM (Fig. 3e), which indicates that stereocilin is a component of a structure located at the interface between the tips of the tallest stereocilia and the TM. Such a structure matches that described previously for the TM-attachment links. In *Tecta*$^{\Delta ENT/\Delta ENT}$ mice that lack alpha-tectorin and all other known non-collagenous glycoproteins of the TM (Legan et al., 2000), the TM is completely detached from the surface of the organ of Corti (Legan et al., 2000). Notably, ring-shaped stereocilin labeling at the tips of the tallest stereocilia was not detected in *Tecta*$^{\Delta ENT/\Delta ENT}$ mice (Fig. 3f), whereas immunogold SEM labeling of the stereocilia from the middle and short rows was still present. However, some gold particles were still detected at the apex of the tallest row, mostly between the tips of the stereocilia, but also on their tips (Fig. 3f). Immunofluorescence stereocilin labeling of all three rows of stereocilia persisted in these mice (Fig. 3g). Together, these results indicate that stereocilin is associated with two types of links in the OHC hair bundle, namely the TM-attachment links and the horizontal top connectors.

We then explored the cochlear distribution of stereocilin in five different mouse models of Usher syndrome type 1 (USH1), a human disease characterized by congenital deafness, vestibular dysfunction and retinitis pigmentosa leading to blindness. Five *USH1* genes involved in different genetic forms of USH1 have been identified, and we explored one mouse model for each of these genetic forms. These mouse mutants are defective for myosin VIIa (*Myo7a*$^{4626SB/4626SB}$ (Mburu et al., 1997), model of USH1B), harmonin (*Ush1c*$^{-/-}$ (Lefèvre et al., 2008)), cadherin 23 (*Cdh23*$^{v2j/v2j}$ (Di Palma et al., 2001; Wilson et al., 2001), model of USH1D), protocadherin 15 (*Pcdh15*$^{av3j/av3j}$ (Alagramam et al., 2001), model of USH1F), or sans (*Ush1g*$^{-/-}$, Caberlotto et al., manuscript in preparation). All have misoriented and fragmented hair bundles (Lefèvre et al., 2008), as a result of the absence or sparsening of transient lateral links that connect stereocilia together and with the kinocilium during early hair-bundle development (Goodyear et al., 2005; Petit and Richardson, 2009). These transient lateral links are composed of cadherin 23 and most likely also by protocadherin 15, and are anchored by harmonin and sans to the stereocilia actin core. In all *Ush1* mutants, a strong stereocilin fluorescent labeling, more intense than in control mice, was observed in mature OHCs, both at the apical end of the tallest stereocilia and between adjacent stereocilia (Fig. 4). This latter labeling encompassed the upper one third to two-thirds of the stereocilia length, instead of being restricted to a small apical region (especially in the tallest stereocilia row) as in the wild-type mice. Expansion of the stereocilin labeling between stereocilia in all *Ush1* mutants was correlated with an extended distribution of lateral links towards the base of stereocilia (see an example in Fig. 4i), as observed by SEM. These results confirm the association of stereocilin with the mature lateral links, i.e. the horizontal top connectors, and suggest that the restricted location of these links to a small distal region depends on the presence of early transient lateral links. In SEM experiments, fibrous material that may correspond to fragments of TM was frequently observed linking the tallest stereocilia of the OHC hair bundle in the *Ush1* mutants (Fig. 4l). Moreover, fluorescent labeling of actin revealed numerous stereocilia clung to the TM when it was removed from the mutants (not shown). These results, related to the very strong stereocilin fluorescent labeling at the very tip of the tallest stereocilia (Fig. 4a-k) indicate that an increased amount of stereocilin at the apical end of the tallest OHC stereocilia strengthens the physical coupling between the hair bundle and the TM, thereby confirming the involvement of stereocilin in this coupling.

Structure of the OHC hair bundle and its coupling to the tectorial membrane in stereocilin-null mice

We studied the structure of the OHC hair bundles and their interaction with the tectorial membrane in *Strc*$^{-/-}$ mice during post-natal cochlear development and until 5 months of age, using SEM and TEM. In IHCs, normal hair bundles were found in *Strc*$^{-/-}$, *Strc*$^{+/-}$, and *Strc*$^{+/+}$ mice at all stages analyzed (not shown). No structural anomalies of *Strc*$^{-/-}$ OHC hair bundles could be detected up to P9 (Fig. 5a, b, d, e). Accordingly, normal mechanoelectrical transduction currents could be recorded in IHCs and OHCs from P7 and P8 stereocilin-null mice (Fig. 6). In *Strc*$^{+/+}$ and *Strc*$^{+/-}$ (Fig. 5e) mice, a large amorphous structure covering the tallest row of OHC stereocilia was observed between P7 and P10 (Fig. 5e). This transient structure, which has already been reported in the rat and in the cat (Ross, 1974; Lenoir et al., 1987; Lim, 1987), sometimes covered several adjacent OHC bundles together, or was seen hanging from the underside of the developing TM (Fig. 7a, b) (Ross, 1974; Lim, 1987). This material was not stereocilin-immunoreactive (Fig. 7c) and was absent in *Strc*$^{-/-}$ mice (Fig. 5b). In the *Strc*$^{-/-}$ mice, the first hair-bundle morphological anomalies were detected in some OHCs at P10. Some stereocilia were disconnected from their neighbors within rows (Fig. 5c). At P11, disconnected stereocilia were present in all *Strc*$^{-/-}$ OHC hair bundles (not shown). At P14, SEM top views showed a loose connection of the stereocilia of the whole OHC bundle in *Strc*$^{-/-}$ mice (Fig. 5g). Compared to the *Strc*$^{+/-}$ hair bundles (Fig. 5j) the

tops of the stereocilia were less clearly aligned. Medial views showed a complete absence of top connectors in P14 *Strc*$^{-/-}$ OHCs, whereas the tip links, which are hardly detectable in control mice, were clearly observed (Fig. 5i, l). Thereafter, the architecture of OHC hair bundles gradually worsened, such that at P60, almost all OHC stereocilia were fully disconnected from their neighbors (Fig. 5m-o) and intact tip links were rarely observed. In the basal, high-frequency-coding region of the cochlea, all OHCs had missing or shortened stereocilia, while in the apical, low-frequency-coding region of the cochlea, the length of stereocilia was still unaffected. At 5 months of age, the basal region of the organ of Corti was severely affected in *Strc*$^{-/-}$ mice compared to the *Strc*$^{+/-}$ control mice: only rare OHC hair bundles, all with scarce and shortened stereocilia, could still be identified. On the other hand, in the apical-end of the cochlea, OHC loss in *Strc*$^{-/-}$ mice was not increased compared to control mice and three rows of stereocilia, some being shortened, were still observed in most OHCs (data not shown). The progressive appearance, after the full disconnection of stereocilia (when the tip links are lost), of shortened stereocilia, in a decreasing number from the base to the apex of the cochlea, suggests that fully disconnected stereocilia brake under the effect of the mechanical forces that are applied to the OHC hair bundle during sound-exposure.

The cochlear microphonic potential is a phasic response reflecting mechanoelectrical transducer currents from basal-coil OHCs. We found that their waveforms have the same amplitude and phase relative to sound in P14 *Strc*$^{-/-}$ and control mice (Verpy et al., 2008), suggesting preserved mechanical coupling between the TM and the organ of Corti in *Strc*$^{-/-}$mice. In these animals, the TM is attached to the spiral limbus (Fig. 8a) and extends throughout the surface of the organ of Corti, as in wild-type mice. Hensen's stripe, a longitudinal ridge on the underside of the TM that has been shown to be attached to the reticular lamina just inside of the IHCs in the guinea pig (Lim, 1972; Ulfendahl et al., 2001), is present and unaffected (Fig. 8a, b), suggesting a normal physical coupling of the TM and reticular lamina in the vicinity of the IHCs. V-shaped rows of dimples (hair-bundle imprints) that correspond to the anchoring points of the OHCs' individual tallest stereocilia on the lower surface of the TM in wild-type and *Strc*$^{+/-}$ mice (Fig. 8c) were, however, absent in *Strc*$^{-/-}$mice (more than 20 cochleae observed, Fig. 8d) by SEM. Since an electron dense granular structure forming a crown at the tips of the OHCs' tallest stereocilia (Tsuprun and Santi, 1998, 2002) has been proposed to mediate TM attachment, we looked for the presence of this crown in *Strc*$^{-/-}$ mice and in *Tecta*$^{\Delta ENT/\Delta ENT}$ mice. The crown could not be detected in *Strc*$^{-/-}$mice (Fig. 8e), but was present in *Tecta*$^{\Delta ENT/\Delta ENT}$ mice (Fig. 8f) in which the stereocilin-immunoreactive ring is absent, thus ruling out the possibility that the electron-dense crown and the stereocilin-immunoreactive ring-shaped structure are identical.

DISCUSSION

A stereocilin-containing structure sheathes the kinocilia of cochlear OHCs and vestibular hair cells

Vestibular hair cells and cochlear OHCs display stereocilin labeling all along their kinocilia from E15.5 and P2 onwards, respectively. In whole-mount preparations of both sensory organs with overlying acellular gels removed, the labeling extends further than the microtubular kinociliary structure. Stereocilin may be a component of a kinocilium-ensheathing structure that couples the kinocilium to the acellular gels (Fig. 9a) and this structure is possibly stretched when the acellular membranes are removed. The pattern of stereocilin labeling on the TM undersurface at P5 suggests that the coupling of the OHC bundle to the TM initially involves the kinocilia of the third row of OHCs. The absence of stereocilin in the vestibular end organs of *Strc*$^{-/-}$ mice does not have a major effect on the anchoring of the acellular membranes to the underlying sensory epithelia, and balance tests (Steel and Hardisty, 1996) that were carried out in these animals did not reveal any

vestibular dysfunction (not shown). This is not surprising as the otoconial membranes and cupulae are secured to the surface of the sensory epithelia by a dense network of filaments that is connected to the apical ends of the supporting cells (Dohlman, 1971; Lim, 1973, 1979; Kachar et al., 1990). A subtle role for stereocilin in directly coupling vestibular hair bundles to the overlying acellular gels cannot, however, be excluded.

Stereocilin is involved in the attachment of the OHC hair bundle to the tectorial membrane

Two lines of evidence indicate stereocilin is required to link the tectorial membrane to the tallest stereocilia of the OHC hair bundle. First, it is associated with the tips of the tallest stereocilia and with the V-shaped arrays of stereociliary imprints that are found in the lower surface of the TM. Second, these imprints and the amorphous extracellular material that covers the tops of the OHC stereocilia from P7 to P10 are both absent in the *Strc*$^{-/-}$ mouse. Moreover, an increased amount of stereocilin at the tip of the tallest OHC stereocilia in *Ush1* mutants seems to strengthen the physical coupling between the OHC hair bundle and the TM.

Although TM attachment crowns are also absent from the *Strc*$^{-/-}$ mouse, various lines of evidence indicate stereocilin is unlikely to be the only component of this structure. First, whilst the ring of stereocilin observed at the tips of the stereocilia resembles the array of electron-dense granules seen at TM attachment sites in the adult chinchilla cochlea following cuprolinic blue treatment (Tsuprun and Santi, 1998, 2002) or in mature mouse cochlear tissues fixed in the presence of tannic acid (Goodyear et al., 2005), such granules are not associated with the stereociliary imprints in the TM (Tsuprun and Santi, 1998) where stereocilin is also present. Second, the expression profile of stereocilin in the developing cochlea does not correlate with the known distribution of attachment crowns. These features are found at the tips of all three rows of stereocilia during cochlear development starting from P2 before becoming gradually restricted to the tallest row (Goodyear et al., 2005). The initial appearance of crowns therefore precedes the first appearance, at P10, of stereocilin in the second and third rows of stereocilia.

Stereocilin may therefore mediate attachment of the OHC hair bundle to both the developing and the mature TM, but is unlikely to be the sole component of the attachment crowns that have been described previously. Furthermore, it can be noted that whilst crowns are present in the *Tecta*$^{\Delta ENT/\Delta ENT}$ mutant mouse, a distinct ring-like pattern of stereocilin labeling is absent from the tip of the stereocilium. Whilst the crowns in the *Tecta*$^{\Delta ENT/\Delta ENT}$ mutant mouse may have some stereocilin associated with them, it is clearly not as organized as it would be in the presence of a tectorial membrane. The TM may therefore recruit stereocilin to the crown and/or organize it within this structure. At the same time, the complete absence of crowns from the hair bundles of mature *Strc*$^{-/-}$ mice indicates that the crowns themselves must require stereocilin for their long-term stability.

Together these finding suggest stereocilin is a protein that links the attachment crown of the stereocilium to the TM. In this respect it is tempting to speculate that stereocilin forms the long, filamentous, antennae-like structures that have been described in guinea-pig OHCs using low-voltage field-emission SEM of non-coated tissues (Dunnebier et al., 1995; Jongebloed et al., 1996; Jongebloed et al., 1999).

The absence of attachment crowns and the lack of stereocilia imprints on the lower surface of the TM in *Strc*$^{-/-}$ mice suggest that, in the absence of stereocilin, the tallest OHC stereocilia are not firmly attached to the TM underside. However, analysis of microphonic potential waveforms indicated preserved mechanical coupling between the TM and OHCs in P14 *Strc*$^{-/-}$ mice (Verpy et al., 2008). This suggests that the TM only acts as a mass load against which the OHC hair bundle can react to boost the displacement of the basilar

membrane. Thus, the direct physical attachment of the OHC hair bundle to the TM would not be critical for correct sound-evoked stimulation of the OHCs. This, however, does not exclude a role for this attachment in the maintenance of OHC / TM mechanical coupling in the long term, or in limiting the magnitude of hair bundle motion in case of sound-overstimulation.

Stereocilin-containing horizontal top connectors maintain the cohesion of the mature OHC hair bundle

We have already reported that stereocilin was associated with the horizontal top connectors in the mature OHCs of the P14 mouse and that these links were absent in P14 *Strc*$^{-/-}$ mice (Verpy et al., 2008). These OHC lateral links, also called side links in other species, have a zipper-like appearance, due to the presence of a tannic acid-reactive medial density, which seems to associate the lateral links in bands (Osborne et al., 1988; Tsuprun and Santi, 1998, 2002; Tsuprun et al., 2003; Goodyear et al., 2005). In the present study, analysis of the stereocilin distribution in wild-type mice during development, and in mature *Ush1* mice, as well as the developmental study of the OHC hair bundle morphology in *Strc*$^{-/-}$ mice confirmed that stereocilin is a component of the horizontal top connectors. Indeed, anti-stereocilin antibodies labeled the lateral links both located between the stereocilia within a row and between the stereocilia from adjacent rows. Notably, the expansion of the stereocilin labeling between adjacent stereocilia in the *Ush1* mature OHCs was correlated with an expanded distribution of the lateral links towards the base of stereocilia. Moreover, whereas the time of appearance of the lateral links fluorescent labeling on the tallest row of stereocilia could not be determined (due to the presence of the attachment links labeling), the appearance of the labeling on the middle and short rows of stereocilia between P10 and P12 is in agreement with the kinetics of horizontal top connector formation (Goodyear et al., 2005). Indeed, these links first appear at P9 in the mouse, concomitantly with the loss of the transient ankle links that connect stereocilia in the differentiating hair bundle, and they attain their zipper-like mature appearance between P12 and P14 (Goodyear et al., 2005). Finally, horizontal top connectors do not form in *Strc*$^{-/-}$ mice.

The resolution of our immunogold labeling experiments was not sufficient to enable precise localization of stereocilin within the bands of top connectors. Stereocilin may be the main component of the central density of horizontal top connectors. In agreement with our proposal, this medial density has not been reported in either IHC or vestibular hair bundles, whose lateral links are not labeled by anti-stereocilin antibodies.

In P14 *Strc*$^{-/-}$ mice, which have almost normal cochlear sensitivity and frequency tuning (Verpy et al., 2008), tip links are present and are the only inter-stereocilia links detected in OHCs. From P15 on, progressive hearing loss occurred in *Strc*$^{-/-}$ mice, and cochlear microphonic recordings indicated a progressive loss of functional mechanoelectrical transducer channels in these animals between P15 and P60 (Verpy et al., 2008). SEM study of *Strc*$^{-/-}$ OHC between P15 and P60 revealed a progressive increase in the number of disconnected stereocilia tips. This suggests a progressive disappearance of the tip links from P15 onwards, which is consistent with the decreasing numbers of tip links that were actually observed in these mice as age increased. As the exposure of P14 mice to a 95 dB SPL pure tone for 10 min induced the same degree of reversible auditory fatigue in control and mutant mice (author's and Paul Avan's (Université d'Auvergne, Clermont-Ferrand, France) unpublished data), it is unlikely that mechanical fragility of the OHC hair bundle is increased in the absence of top connectors only (when tip links are still present). We thus suggest that horizontal top connectors, by maintaining the tips of the stereocilia from the middle and short rows in close proximity with the stereocilia shafts of the tallest and middle rows, respectively, may assist the normal turn over of the tip links.

Supplementary Material

Refer to Web version on PubMed Central for supplementary material.

Acknowledgments

All confocal and SEM images were acquired at the Institut Pasteur's Plate-Forme d'Imagerie Dynamique and Plate-Forme de Microscopie Ultrastructurale, respectively. We are grateful to Pr. Paul Avan for testing the susceptibility of *Strc*$^{-/-}$ mice to noise exposure, and to Dr. Jean-Pierre Hardelin for critical reading of the manuscript. We also thank Isabelle Perfettini, Emilie Bizard and Isabelle Palacios for technical help.

Funded by : - European Commission FP6 Integrated Project EuroHear ; Grant Number LSHG-CT-2004-512063

- Fondation Raymonde & Guy Strittmatter – Fondation de France

- Société Réunica-Prévoyance

- The Wellcome Trust ; Grant Number 071394/Z/03/Z

LITERATURE CITED

Alagramam KN, Murcia CL, Kwon HY, Pawlowski KS, Wright CG, Woychik RP. The mouse Ames waltzer hearing-loss mutant is caused by mutation of Pcdh15, a novel protocadherin gene. Nat Genet. 2001; 27:99–102. [PubMed: 11138007]

Ashmore JF. A fast motile response in guinea-pig outer hair cells: the cellular basis of the cochlear amplifier. J Physiol. 1987; 388:323–347. [PubMed: 3656195]

Brownell WE, Bader CR, Bertrand D, de Ribaupierre Y. Evoked mechanical responses of isolated cochlear outer hair cells. Science. 1985; 227:194–196. [PubMed: 3966153]

Delgutte, B. Physiological models for basic auditory percepts. In: Hawkins, HH.; McMullen, TA.; Popper, AN.; Fay, RR., editors. Auditory Computation. Springer; New York: 1996. p. 157-220.

Di Palma F, Holme RH, Bryda EC, Belyantseva IA, Pellegrino R, Kachar B, Steel KP, Noben-Trauth K. Mutations in Cdh23, encoding a new type of cadherin, cause stereocilia disorganization in waltzer, the mouse model for Usher syndrome type 1D. Nat Genet. 2001; 27:103–107. [PubMed: 11138008]

Dohlman GF. The attachment of the cupulae, otolith and tectorial membranes to the sensory cell areas. Acta Otolaryngol. 1971; 71:89–105. [PubMed: 4102724]

Dunnebier EA, Segenhout JM, Kalicharan D, Jongebloed WL, Wit HP, Albers FW. Low-voltage field-emission scanning electron microscopy of non-coated guinea-pig hair cell stereocilia. Hear Res. 1995; 90:139–148. [PubMed: 8974991]

Furness DN, Hackney CM. Cross-links between stereocilia in the guinea pig cochlea. Hear Res. 1985; 18:177–188. [PubMed: 4044419]

Goldstein JL. Auditory nonlinearity. J Acoust Soc Am. 1967; 41:676–689. [PubMed: 6045077]

Goodyear RJ, Marcotti W, Kros CJ, Richardson GP. Development and properties of stereociliary link types in hair cells of the mouse cochlea. J Comp Neurol. 2005; 485:75–85. [PubMed: 15776440]

Jongebloed WL, Dunnebier EA, Albers FW, Kalicharan D. Demonstration of the fine structure of stereocilia in the organ of Corti of the guinea pig by field emission scanning electron microscopy. Scanning Microsc. 1996; 10:147–163. discussion 163-144. [PubMed: 9813603]

Jongebloed WL, Stokroos I, Van der Want JJ, Kalicharan D. Non-coating fixation techniques or redundancy of conductive coating, low kV FE-SEM operation and combined SEM/TEM of biological tissues. J Microsc. 1999; 193:158–170. [PubMed: 10048219]

Kachar B, Parakkal M, Fex J. Structural basis for mechanical transduction in the frog vestibular sensory apparatus: I. The otolithic membrane. Hear Res. 1990; 45:179–190. [PubMed: 2358412]

Kemp DT. Stimulated acoustic emissions from within the human auditory system. J Acoust Soc Am. 1978; 64:1386–1391. [PubMed: 744838]

Kennedy HJ, Crawford AC, Fettiplace R. Force generation by mammalian hair bundles supports a role in cochlear amplification. Nature. 2005; 433:880–883. [PubMed: 15696193]

Kozlov AS, Risler T, Hudspeth AJ. Coherent motion of stereocilia assures the concerted gating of hair-cell transduction channels. Nat Neurosci. 2007; 10:87–92. [PubMed: 17173047]

Lefèvre G, Michel V, Weil D, Lepelletier L, Bizard E, Wolfrum U, Hardelin JP, Petit C. A core cochlear phenotype in USH1 mouse mutants implicates fibrous links of the hair bundle in its cohesion, orientation and differential growth. Development. 2008; 135:1427–1437. [PubMed: 18339676]

Legan PK, Lukashkina VA, Goodyear RJ, Kossi M, Russell IJ, Richardson GP. A targeted deletion in alpha-tectorin reveals that the tectorial membrane is required for the gain and timing of cochlear feedback. Neuron. 2000; 28:273–285. [PubMed: 11087000]

Lenoir M, Puel JL, Pujol R. Stereocilia and tectorial membrane development in the rat cochlea. A SEM study. Anat Embryol (Berl). 1987; 175:477–487. [PubMed: 3578826]

Lim DJ. Fine morphology of the tectorial membrane. Its relationship to the organ of Corti. Arch Otolaryngol. 1972; 96:199–215. [PubMed: 4628258]

Lim DJ. Ultrastructure of the otolithic membrane and the cupula. A scanning electron microscopic observation. Adv Otorhinolaryngol. 1973; 19:35–49. [PubMed: 4198042]

Lim DJ. Fine morphology of the otoconial membrane and its relationship to the sensory epithelium. Scan Electron Microsc. 1979:929–938. [PubMed: 524064]

Lim DJ. Development of the tectorial membrane. Hear Res. 1987; 28:9–21. [PubMed: 3610861]

Mburu P, Liu XZ, Walsh J, Saw D Jr. Cope MJ, Gibson F, Kendrick-Jones J, Steel KP, Brown SD. Mutation analysis of the mouse myosin VIIA deafness gene. Genes Funct. 1997; 1:191–203. [PubMed: 9680294]

Michalski N, Michel V, Bahloul A, Lefevre G, Barral J, Yagi H, Chardenoux S, Weil D, Martin P, Hardelin JP, Sato M, Petit C. Molecular characterization of the ankle-link complex in cochlear hair cells and its role in the hair bundle functioning. J Neurosci. 2007; 27:6478–6488. [PubMed: 17567809]

Michel V, Goodyear RJ, Weil D, Marcotti W, Perfettini I, Wolfrum U, Kros CJ, Richardson GP, Petit C. Cadherin 23 is a component of the transient lateral links in the developing hair bundles of cochlear sensory cells. Dev Biol. 2005; 280:281–294. [PubMed: 15882573]

Osborne MP, Comis SD, Pickles JO. Further observations on the fine structure of tip links between stereocilia of the guinea pig cochlea. Hear Res. 1988; 35:99–108. [PubMed: 3182414]

Petit C, Richardson GP. Linking genes underlying deafness to hair-bundle development and function. Nat Neurosci. 2009; 12:703–710. [PubMed: 19471269]

Ross MD. The tectorial membrane of the rat. Am J Anat. 1974; 139:449–481. [PubMed: 4131837]

Steel, KP.; Hardisty, R. Assessing hearing, vision and balance in mice. In: Neuroscience, Sf, editor. What's wrong with my mouse? New interplays between mouse genes and behavior. Washington D. C.: 1996. p. 26-38.

Tsuprun V, Santi P. Structure of outer hair cell stereocilia links in the chinchilla. J Neurocytol. 1998; 27:517–528. [PubMed: 11246491]

Tsuprun V, Santi P. Structure of outer hair cell stereocilia side and attachment links in the chinchilla cochlea. J Histochem Cytochem. 2002; 50:493–502. [PubMed: 11897802]

Tsuprun V, Schachern PA, Cureoglu S, Paparella M. Structure of the stereocilia side links and morphology of auditory hair bundle in relation to noise exposure in the chinchilla. J Neurocytol. 2003; 32:1117–1128. [PubMed: 15044843]

Ulfendahl M, Flock A, Scarfone E. Structural relationships of the unfixed tectorial membrane. Hear Res. 2001; 151:41–47. [PubMed: 11124450]

Verpy E, Masmoudi S, Zwaenepoel I, Leibovici M, Hutchin TP, Del Castillo I, Nouaille S, Blanchard S, Laine S, Popot JL, Moreno F, Mueller RF, Petit C. Mutations in a new gene encoding a protein of the hair bundle cause non-syndromic deafness at the DFNB16 locus. Nat Genet. 2001; 29:345–349. [PubMed: 11687802]

Verpy E, Weil D, Leibovici M, Goodyear RJ, Hamard G, Houdon C, Lefevre GM, Hardelin JP, Richardson GP, Avan P, Petit C. Stereocilin-deficient mice reveal the origin of cochlear waveform distortions. Nature. 2008; 456:255–258. [PubMed: 18849963]

Wilson SM, Householder DB, Coppola V, Tessarollo L, Fritzsch B, Lee EC, Goss D, Carlson GA, Copeland NG, Jenkins NA. Mutations in Cdh23 cause nonsyndromic hearing loss in waltzer mice. Genomics. 2001; 74:228–233. [PubMed: 11386759]

Europe PMC Funders Author Manuscripts

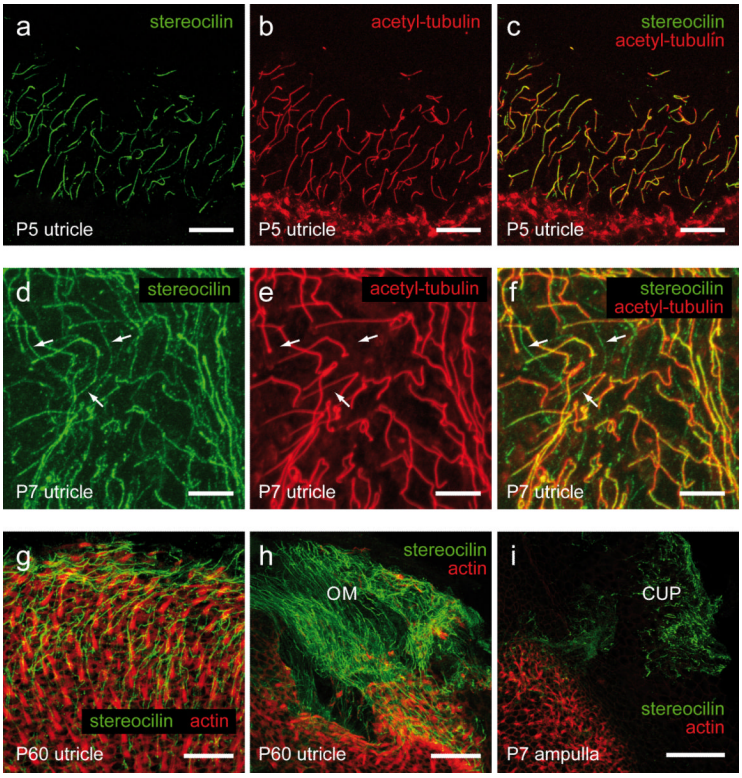

Figure 1.

Stereocilin in the mouse vestibular end organs. Thick cryostat sections **(a-c)** or compressions of z stack confocal images of whole mount preparations (**d-i**) permeabilized with Triton X-100 before immunostaining. Stereocilin was detected in the five vestibular sensory areas. However, the staining was much fainter and more punctate in the ampullae than in the maculae. **(a-c)** P5 utricle stained for stereocilin (green, **a**) and acetyl-tubulin (red, **b**); **c**, merged image. On thick sections, stereocilin staining does not extend beyond the kinocilium. **(d-f)** P7 utricle stained for stereocilin (green, **d**) and acetyl-tubulin (red, **e**), **f**, merged image. Arrows point to the stereocilin staining that extends far beyond the acetyl-tubulin-immunoreactive kinocilium. (**g, h, i**) P60 utricle (**g, h**) and P7 ampulla (**i**) stained for stereocilin (green) and actin (red). Whether the acellular membranes were removed before or after paraformaldehyde-fixation, most of the fiber-like stereocilin staining remained associated with the acellular gels removed from the underlying sensory epithelia (**h, i**). A magenta-green copy of this figure is available as Supplementary Figure 1. Scale bars : 20 μm (a-c, g), 10 μm (d-f), 30 μm (h), and 50 μm (i).

Europe PMC Funders Author Manuscripts

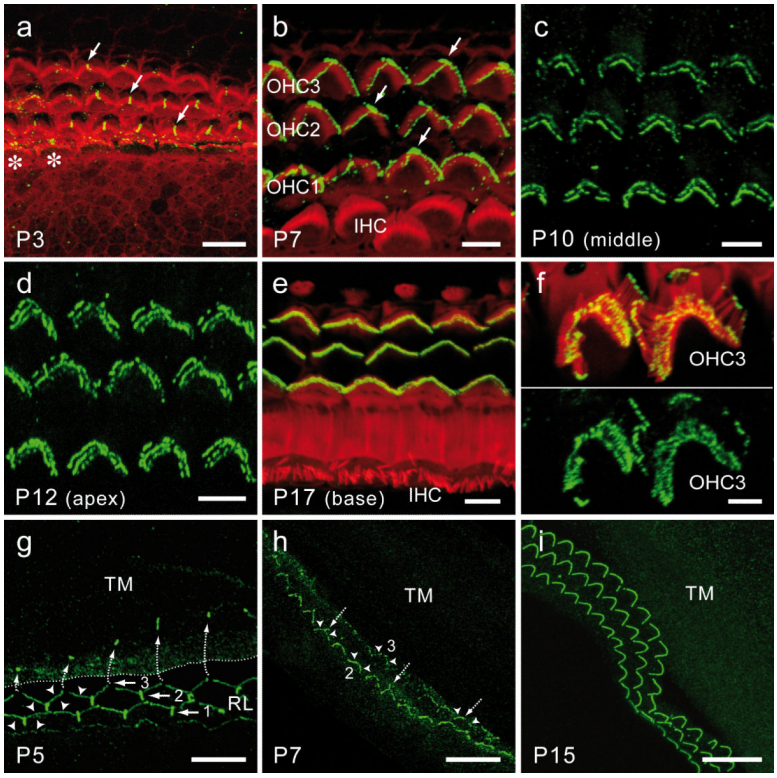

Figure 2.

Stereocilin in the developing cochlea. Confocal images (single stacks or compressions) of whole-mount preparations stained for stereocilin (green) and actin (red). All images were obtained from the mouse, except **f**, which was obtained from the adult guinea-pig. Arrows (**a, b, g)** point to the kinocilium in OHCs from the three rows. This organelle disappears gradually from P7. Asterisks in **a** indicate IHCs with stereocilin staining above their surface in the region of the kinocilium. This staining was also occasionally observed at later stages, when the kinocilium has disappeared, and was not present in *Strc*$^{-/-}$ mice. **g-i** illustrate stereocilin labeling of the developing and mature tectorial membrane (delimited by a dotted line), whose external edge is lifted up and turned up (circular arrow). In **g** and **h**, dotted arrows point to the stereocilin immunolabeling, derived from some kinocilia of the basal third row (at P5 and P7) and second row (at P7) of OHCs. This labeling has lifted off with the tectorial membrane, while the kinocilium is still present in the corresponding OHC hair bundles (not shown). Arrowheads point to the labeling at the tips of the tallest stereocilia from the three rows of OHCs. In the basal region of the P7 cochlea, this labeling is occasionally lifted off from the second (2) and third (3) rows of OHCs and associated with the TM (**h)**. A magenta-green copy of this figure is available as Supplementary Figure 2. Scale bars: 10 μm (a, g), 5 μm (b-e), 2.5 μm (f), 20 μm (h, i).

Europe PMC Funders Author Manuscripts

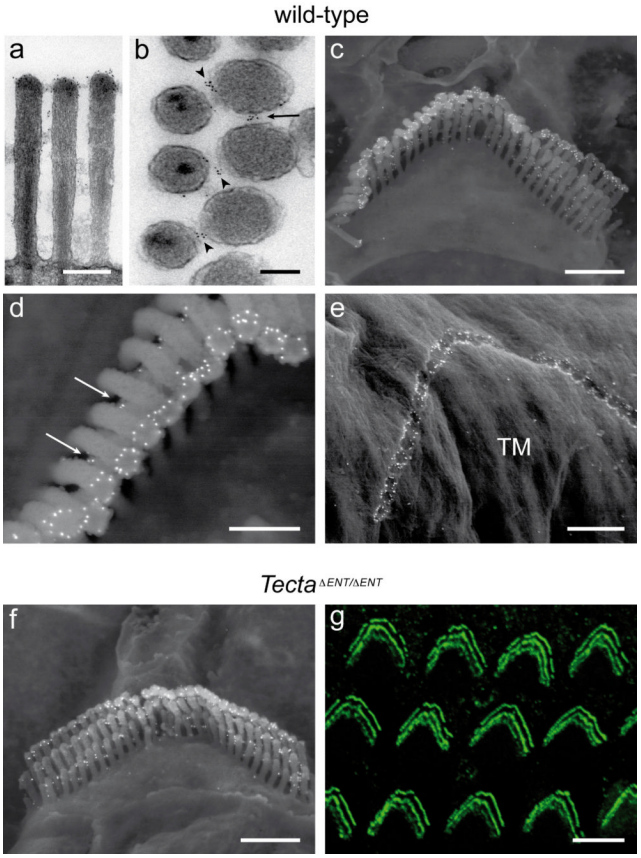

Figure 3.

Two stereocilin-containing structures in the mature OHC bundle. (**a, b**) Transmission electron micrographs of the hair bundles from P22 wild-type OHC after stereocilin immunolabeling. On longitudinal sections of stereocilia in the tallest row (**a**), gold particles are located mainly around the tips of the stereocilia. On horizontal sections (**b**), labeling is associated with the lateral links that connect adjacent stereocilia within a row (arrows) and between rows (arrowheads). (**c-f**) Scanning electron micrographs of P15 OHC bundles (**c, d, f**) and undersurface of the tectorial membrane (**e**) after stereocilin immunolabeling in wild-type (**c-e**) and *Tecta*$^{\Delta ENT/\Delta ENT}$ (**f**) mice. (**g**) Confocal image of P15 *Tecta*$^{\Delta ENT/\Delta ENT}$ OHC hair bundles labeled for stereocilin. In wild-type mice, annular labeling is observed by SEM around the tips of stereocilia from the tallest row (**c, d**) and at the periphery of the stereocilia imprints on the TM underside (**e**). Gold particles are also distributed between adjacent stereocilia located in different rows (arrows in **d**) and in the same row, notably between the tips of stereocilia from the tallest row. In *Tecta*$^{\Delta ENT/\Delta ENT}$ mice with a detached TM, some gold particles are present on the tips of the tallest stereocilia, but a ring-shaped labeling is not observed around these tips (**f**), whereas the labeling between stereocilia of the three rows is maintained (**f, g**). The comparative analysis of the stereocilin distribution in *Tecta*$^{\Delta ENT/\Delta ENT}$ and control mice indicates that, in the mouse, the stereocilin-containing horizontal top connectors that connect adjacent stereocilia in the tallest row are restricted to their tips. Scale bars : 0.2 μm (a, b), 1 μm (c, e, f), 0.5 μm (d) and 5 μm (g).

Europe PMC Funders Author Manuscripts

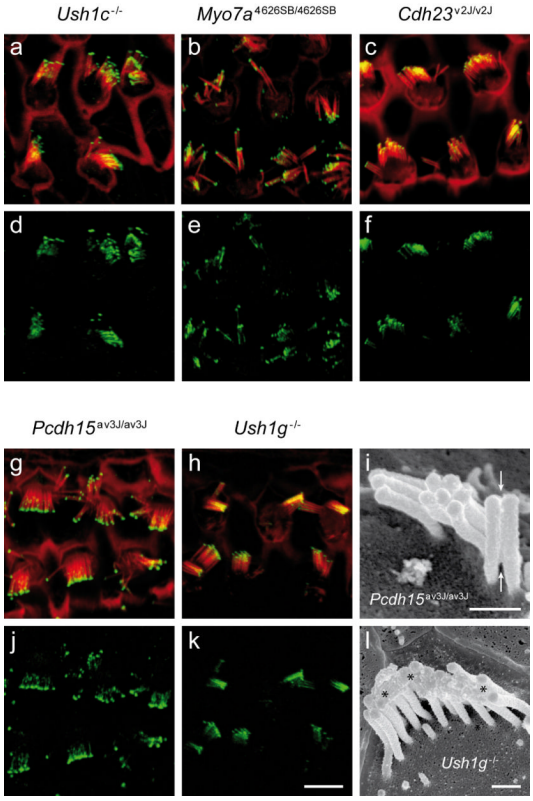

Figure 4.

Expanded distributions of stereocilin-associated links in *Ush1* mutant mice. (**a-h, j, k**) Confocal images of mature (P14-P40) OHC hair bundles stained for stereocilin (green) and actin (red). In all *Ush1* mutants, the stereocilin labeling is very strong and its distribution is expanded, compared to the wild-type mice. Labeling between stereocilia distributes across the upper two thirds of their length, instead of being restricted to the apical region of stereocilia. (**i, l**) Scanning electron micrographs. In P15 *Pcdh15*$^{av3J/av3J}$ OHC hair bundles, adjacent stereocilia are closely connected by lateral links (between arrows) that extend toward the base of stereocilia. In *Ush1g*$^{-/-}$ OHCs, adjacent stereocilia are connected along their shafts, and their apical ends are linked together by fibrous material (asterisks). A magenta-green copy of this figure is available as Supplementary Figure 3. Scale bars : 5 μm (in k, for all confocal images), and 0. 5 μm (i, l).

Europe PMC Funders Author Manuscripts

Europe PMC Funders Author Manuscripts

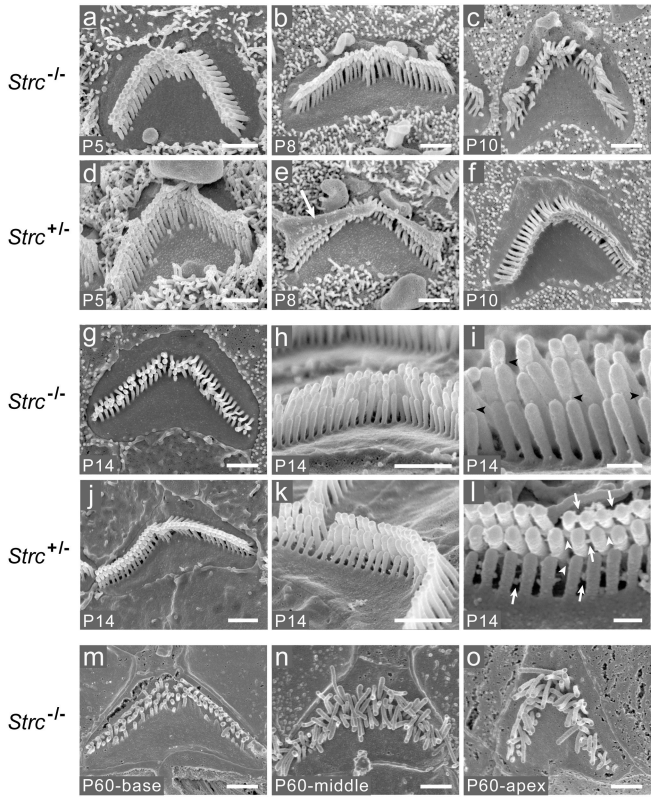

Figure 5.

Scanning electron micrographs of OHC bundles in stereocilin-null mutant mice (**a-c, g-i, m-o**). Normal OHC bundles from heterozygous (*Strc*$^{+/-}$) mice are shown for comparison (**d-f, j-l**). In P5 and P8 stereocilin-null (*Strc*$^{-/-}$) mice, the OHC bundle architecture is still normal (**a, b**). However, a large amorphous structure covering the tallest row of stereocilia in P8 *Strc*$^{+/-}$ mice (arrow in **e**) is absent in *Strc*$^{-/-}$ mice. This is a transient structure, which is observed from P7 and is no longer detected at P11 in normal mice (see Fig. 7). At P10 (**c**), some *Strc*$^{-/-}$ hair bundles display partial loss of cohesiveness, due to the loss of connection of adjacent stereocilia within rows. At P14, top and medial views of OHC bundles show looser connection of stereocilia in *Strc*$^{-/-}$ mice (**g-i**) than in *Strc*$^{+/-}$ mice (**j-l**). On high-magnification micrographs, lateral links that connect adjacent stereocilia both within rows (arrows in **l**) and in different rows (arrowheads in **l**) are not detected in *Strc*$^{-/-}$ mice, whereas tip kinks (arrowheads in **i**) are still present. In P60 *Strc*$^{-/-}$ mice (**m-o**), almost all OHC stereocilia are fully disconnected from their neighbors; a few tip links are still observed, mostly in the apical part of the cochlea (not shown). OHCs from the basal part of the cochlea display fused, broken, and missing stereocilia (**m**). Scale bars: 1 μm (a-h, j, k, m-o), 0.25 μm (i, l).

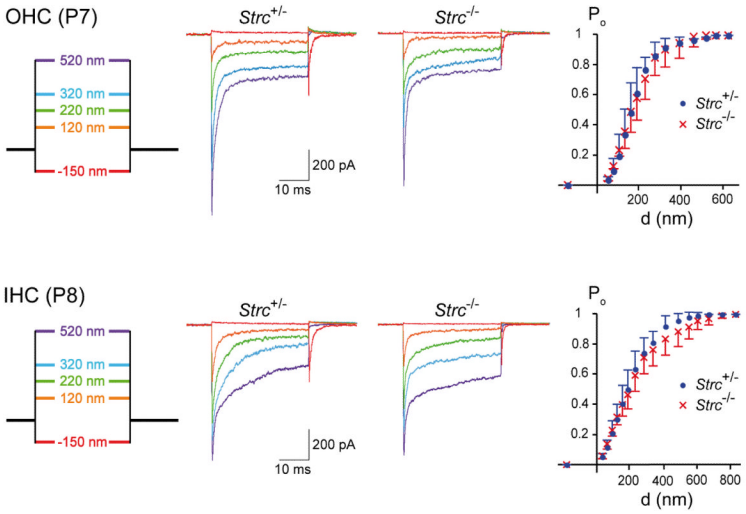

Figure 6.

Mechanoelectrical transduction current recordings in cochlear hair cells from stereocilin-null mice. Mechanoelectrical transduction currents were recorded in OHCs **(a)** and IHCs **(b)** from the apical turn of the cochlea (35-50% from the cochlear apex) of *Strc*$^{+/-}$ and *Strc*$^{-/-}$ mice at P7 or P8 following different hair bundle displacements (indicated on the left). **(c)** Average open probability (Po) +/− s.d. - displacement (d) curves plotted for P7 OHCs and P8 IHCs. No significant difference is observed between *Strc*$^{+/-}$ (n=5) and *Strc*$^{-/-}$ (n=5) mice. The maximal current amplitude was 905±205 pA in *Strc*$^{-/-}$ OHCs (n=15), compared to 754±198 pA in *Strc*$^{+/-}$ OHCs (n=16, Student's t test p=0.09). Fast adaptation was not modified in *Strc*$^{-/-}$ OHCs, with a time constant of 434±184 μs (n=14), compared to 438±144 μs (n=13) in *Strc*$^{+/-}$ OHCs (Student's t test p=0.94). The values varied very little in P8 mice, with a mean maximum amplitude of 1065±233 pA (n=6) and a fast adaptation time constant of 397±143 μs (n=6) in *Strc*$^{-/-}$ mice, compared to 1111±261 pA (n=5) (Student's t test versus mutant mice p=0.79) and 292±129 μs (n=5) (Student's t test versus mutant mice p=0.28) in *Strc*$^{+/-}$ mice, respectively. Mechanoelectrical transduction currents recorded in IHCs from *Strc* $^{-/-}$ and *Strc* +/− P8 mice were also similar, with a mean maximum amplitude of 781±163 pA (n=15) and a fast adaptation time constant of 1163±768 μs (n=15) in *Strc*$^{-/-}$ mice, compared to 787±93 pA (n=13, Student's t test versus mutant mice p=0.91) and 928±539 μs (n=13, Student's t test versus mutant mice p=0.35) in *Strc*$^{+/-}$ mice, respectively.

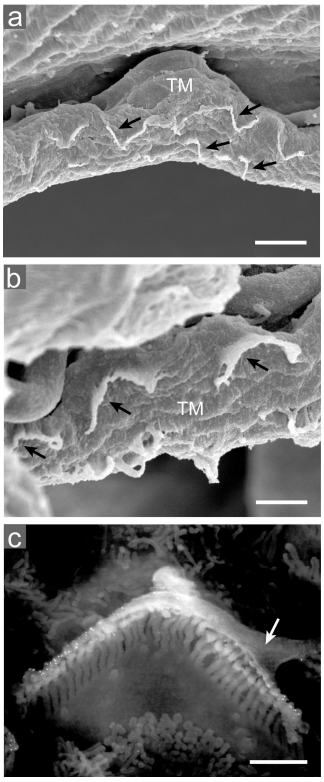

Figure 7.

A transient amorphous structure connecting the OHC hair bundle and the tectorial membrane between P7 and P10. (**a**, **b**) Scanning electron micrographs of the undersurface of the TM in a P8 wild-type mouse. An amorphous structure is hanging from the underside of the developing TM, at the sites where the OHC stereociliary bundles were contacting the membrane (arrows). (**c**) Scanning electron micrograph of a P8 OHC hair bundle after stereocilin immunolabeling. The transient amorphous structure is not labeled by anti-stereocilin antibodies. Scale bars : 3 μm (a), 1.5 μm (b) and 1 μm (c).

Europe PMC Funders Author Manuscripts

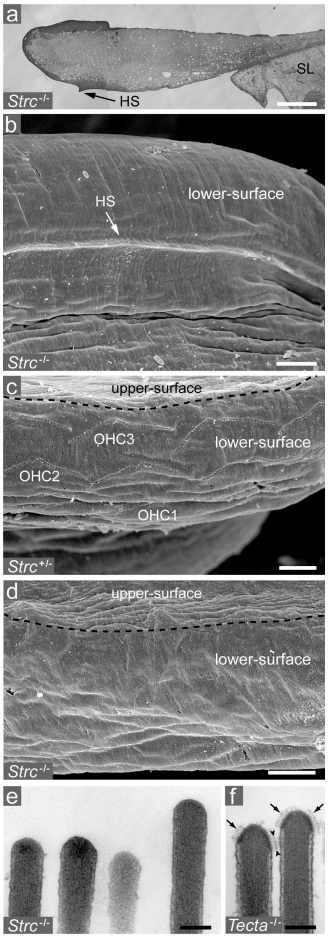

Figure 8.

Tectorial membrane-organ of Corti relationship in *Strc*$^{-/-}$ mice. Transmission electron micrograph (**a**, assembling of 10 micrographs using Photoshop™) and scanning electron micrographs **(b, c, d)** of the TM in 6 week-old *Strc*$^{-/-}$ (**a, b, d**) and *Strc*$^{+/-}$ (**c**) mice. In the *Strc*$^{-/-}$ mouse, the TM is attached to the spiral limbus (SL), and the Hensen stripe (HS) is present on the lower-surface of the TM, as in wild-type mice (**a, b**). Three rows of V-shaped imprints are present on the lower-surface of the TM in *Strc*$^{+/-}$ mice (**c**). These imprints are formed by the notches remaining after the tallest row of OHC stereocilia was pulled away from the TM. Such imprints are not found in the TM of *Strc*$^{-/-}$ mice (**d**). **(e, f)** Transmission electron micrographs of the tallest OHC stereocilia in P14 *Strc*$^{-/-}$ and *Tecta*$^{\Delta ENTT/\Delta ENT}$ (*Tecta*$^{-/-}$) mice. An electron dense granular structure (arrows) forms a crown at the tips of the tallest stereocilia in *Tecta*$^{-/-}$ mice (**f**), but not *Strc*$^{-/-}$ mice (**e**). Arrowheads in **f** delineate a band of horizontal top connectors located just below the crown. Scale bars: 10 μm (a), 5 μm (b), 2.5 μm (c, d) and 200 nm (e, f).

Europe PMC Funders Author Manuscripts

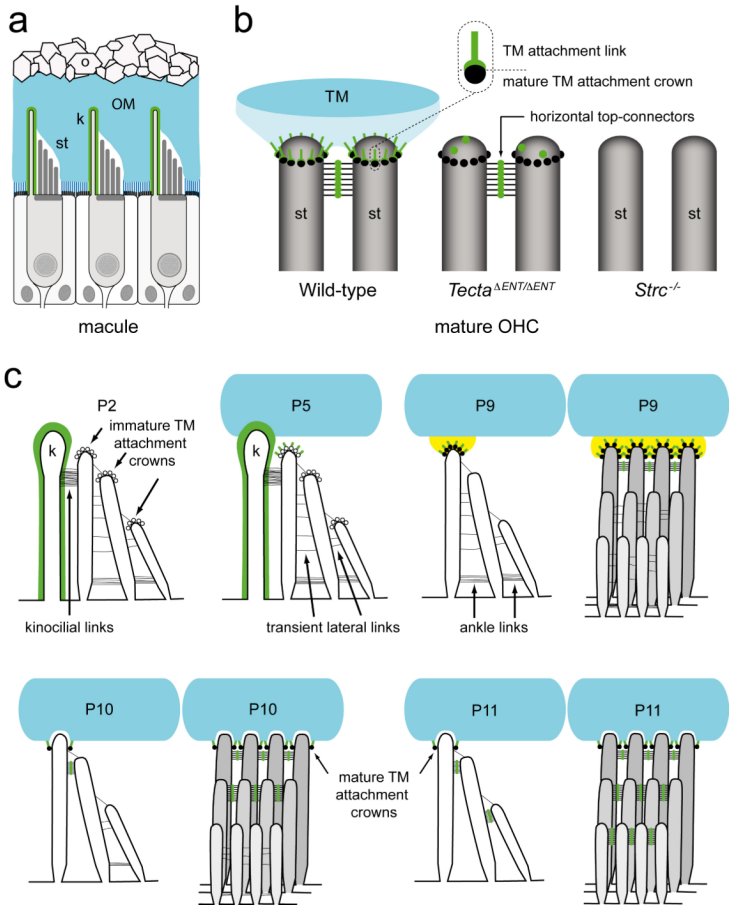

Figure 9.

Proposed roles of stereocilin in the inner ear. Some details provided on this summary illustration are hypothetical. Stereocilin is in green and the vestibular and cochlear acellular gels are in light blue. (**a**) Stereocilin is a component of a structure ensheathing the kinocilium (k). This sheath is likely to be involved in coupling the hair bundles to the acellular gels. The otoconial membranes (OM) of the saccule and utricle are overlaid with dense biominerals, the otoconia (o) and are connected to the apical surface of the supporting cells by a dense network of filaments (in dark blue). st, stereocilia. (**b**) Stereocilin at the tips of the tallest OHC stereocilia. Stereocilin is a component of both the horizontal top connectors and links that attach the tectorial membrane to the tallest stereocilia (TM attachment links). In the mature cochlea, only the tips of the tallest stereocilia (st) of OHCs are anchored in the tectorial membrane (TM). The stereocilin-containing attachment links, represented as an array of umbrella ribs, attach the TM to an anchoring platform composed of electron-dense structures (black circles) forming a crown (TM attachment crown). In the horizontal top connectors, stereocilin is represented as composing the central density, which is still hypothetical. In the *Tecta*$^{\Delta ENT/\Delta ENT}$ mutant mice with detached TM, the TM attachment crown is present, as well as the horizontal top connectors, while the attachment links are absent. The *Strc*$^{-/-}$ mice lack both the attachment links and the horizontal top connectors, and the TM attachment crowns are not detected. **(c)** Stereocilin in developing OHCs. The stages that are indicated refer to the basal region of the cochlea. At P2, stereocilin is only detected along the kinocilium (k). The immature attachment crowns (white circles) are present at the tip of the stereocilia from all three rows. At P5, a coupling between the developing TM and the OHC hair bundles makes use of stereocilin covering the

kinocilium tip. Stereocilin is also present at the tips of the tallest stereocilia. At P9, the kinocilium has disappeared and the presence of stereocilin at the tips of the tallest stereocilia has induced the maturation of the TM attachment crown. The transient amorphous material (in yellow) that couples the TM and OHC hair bundles is attached to the tips of the tallest stereocilia through stereocilin. It is still unknown whether this amorphous material (present between P7 and P9 in the basal part of the cochlea) is an independent structure or is part of the developing TM. The interstereociliary top connectors appear between stereocilia in the tallest row. At P10, the tallest stereocilia are anchored in the TM and the stereocilin-containing attachment links attach the TM attachment crowns to the TM, while the stereocilin-containing top connectors appear both between stereocilia in the middle row and between stereocilia from the tall and middle rows. At P11, top connectors are also present between stereocilia in the small row and between stereocilia from the middle and small rows.

Europe PMC Funders Author Manuscripts

Europe PMC Funders Author Manuscripts

Antigen	Immunogen	Manufacturer, species antibody was raised in, mono- vs. polyclonal, catalog or lot number	Dilution used
Acetylated tubulin	Acetylated tubulin from outer arm of sea urchin sperm axonem	Sigma-Aldrich, mouse monoclonal, clone 6-11B-1, #T7451	1:300
Stereocilin	Synthetic peptide, aa 970-985 from N-terminus (mouse)	Rabbit polyclonal, affinity-purified	1:150 (1.4 μg/ml)
Stereocilin	Synthetic peptide, aa 1753-1767 from N-terminus (mouse)	Rabbit polyclonal, affinity-purified	1:50 (2.3 μg/ml)